Research Article

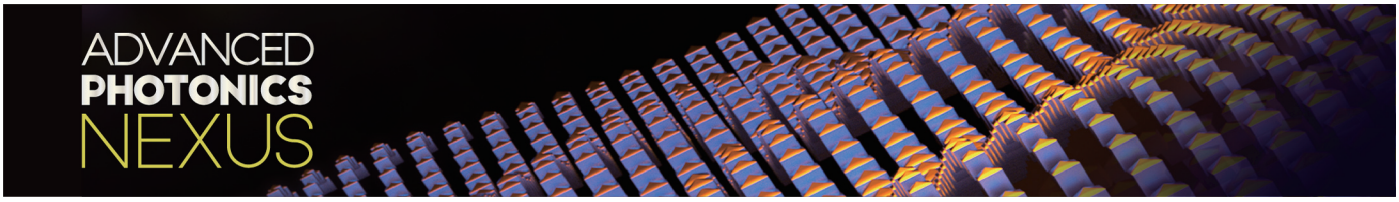

Uniformly polarized multi-output illumination by metasurfaces performing near-complete conversion of unpolarized light

Neuton Li,[a,*] Jihua Zhang,[a,b] Shaun Lung,[a,c] Dragomir N. Neshev,[a] and Andrey A. Sukhorukov[a,*]
[a]Australian National University, Research School of Physics, ARC Centre of Excellence for Transformative Meta-Optical Systems, Department of Electronic Materials Engineering, Canberra, Australia
[b]Songshan Lake Materials Laboratory, Dongguan, China
[c]Friedrich-Schiller University, Institute of Applied Physics, Jena, Germany

Abstract. Many technologies, including dot projectors and lidar systems, benefit greatly from using polarized illumination. However, conventional polarizers and polarizing beam splitters have a fundamental limit of 50% efficiency when converting unpolarized light into one specific polarization. Here, we overcome this restriction and achieve near-complete conversion of unpolarized light to a spatially uniform polarization state over several output directions with our topology-optimized metasurfaces. Our results provide a path toward greatly improving the efficiency of common unpolarized light sources, such as LEDs, for a variety of applications requiring uniformly polarized illumination. Our fabricated metasurface realizes a 70% conversion efficiency, surpassing the aforementioned limit, and achieves a polarization extinction ratio exceeding 20, when characterized with laboratory measurements. We further demonstrate that arbitrary power splitting can be achieved between three or more polarized outputs, offering flexibility in target illumination.

Keywords: metasurfaces; polarization; diffraction; topology optimization.

Received Jun. 13, 2024; revised manuscript received Aug. 1, 2024; accepted for publication Aug. 27, 2024; published online Sep. 23, 2024.

[DOI: 10.1117/1.APN.3.6.066002]

1 Introduction

Polarization is a fundamental property of light that can carry and probe information with a wide range of applications including imaging,[1–3] sensing,[4,5] and communications,[6,7] which often benefit from having a predefined pure polarization state as the input or output. For example, structured dot-array patterns for depth imaging combined with polarized illumination and detection allow one to distinguish between specular and diffuse reflections,[8] where highly polarized laser arrays are required. Remarkably, our approach can enable such schemes to efficiently operate using unpolarized sources, such as LEDs, combined with specially designed metasurfaces that convert greater than 80% of all unpolarized light to a particular polarization across multiple dot-array outputs, enabling broader penetration of advanced imaging technologies in end-user devices.

Whereas lasers with a polarized output are available, the cheaper and more ubiquitous sources such as LEDs usually emit unpolarized or partially polarized light. Efficient extraction of fully polarized light from such sources remains a challenging problem.[9–11] The traditional approach is to filter out the undesired orthogonal state with a linear polarizer, sometimes in combination with wave plates if the target polarization is elliptical or circular.[12] This process is energy inefficient, since there is a 50% limit for conversion of unpolarized to fully polarized light with conventional polarizers.[13] If this limit were to be surpassed in a compact form factor, greater flexibility would be achieved in optical devices for various applications requiring uniformly polarized illumination simultaneously in multiple spatial directions.

In the last decade, there have been great advances in shaping polarization states of light with optical metasurfaces, composed

*Address all correspondence to Neuton Li, Neuton. Li@anu.edu.au; Andrey A. Sukhorukov, Andrey. Sukhorukov@anu.edu.au

of a planar array of nanostructures with subwavelength thicknesses.[14–20] A single metasurface can enable arbitrary polarization conversion and dichroism to realize the functions of wave plates and polarizers.[21–24] Metasurface holograms that combine different polarizing meta-atoms into an array can be used as a polarimeter by projecting different states into spatially distinct regions.[25–28] In addition, recent work has demonstrated the ability to control the degree of polarization with a metasurface by filtering unpolarized incident light to arbitrary partially or fully polarized output.[29] However, all of these pillar-based metasurfaces are still fundamentally limited to the 50% conversion efficiency when polarizing unpolarized light. We discuss the reasoning for this limitation in Sec. 2.2. Metasurfaces have also replicated and extended the functionality of a conventional polarizing beam splitter (PBS)[28,30–34] by splitting incoming light into multiple pairs of orthogonally polarized beams, as illustrated on a Poincaré sphere in Fig. 1(a). The PBS is an energy-efficient approach, directing orthogonal linear polarizations into separate paths. Though the total transmitted power is conserved, the resulting beams are, however, not of the same polarization. To obtain the desired spatially uniform polarization, additional wave plates are required. This additional bulk and complexity would be incompatible with compact end-user devices requiring integrated optical solutions.

In this work, we reveal, for the first time to our knowledge, the ultimate efficiency and flexibility in converting an unpolarized input state to a spatially uniform output polarization state. This is achieved through specially designed elements with multiple output channels, thus overcoming the efficiency limit of a single-output polarizer [Fig. 1(b)]. We implement this principle by inversely designing metasurfaces with two, three, and four outputs. Each can convert unpolarized light into a single predefined output polarization state with combined efficiency far exceeding the 50% threshold, such that the polarization state is spatially uniform across all the output directions. In experiments, we demonstrate the dual-output metasurface polarizer, with the measured efficiency reaching 70%, thus demonstrating the practical feasibility of our concept. These fundamental

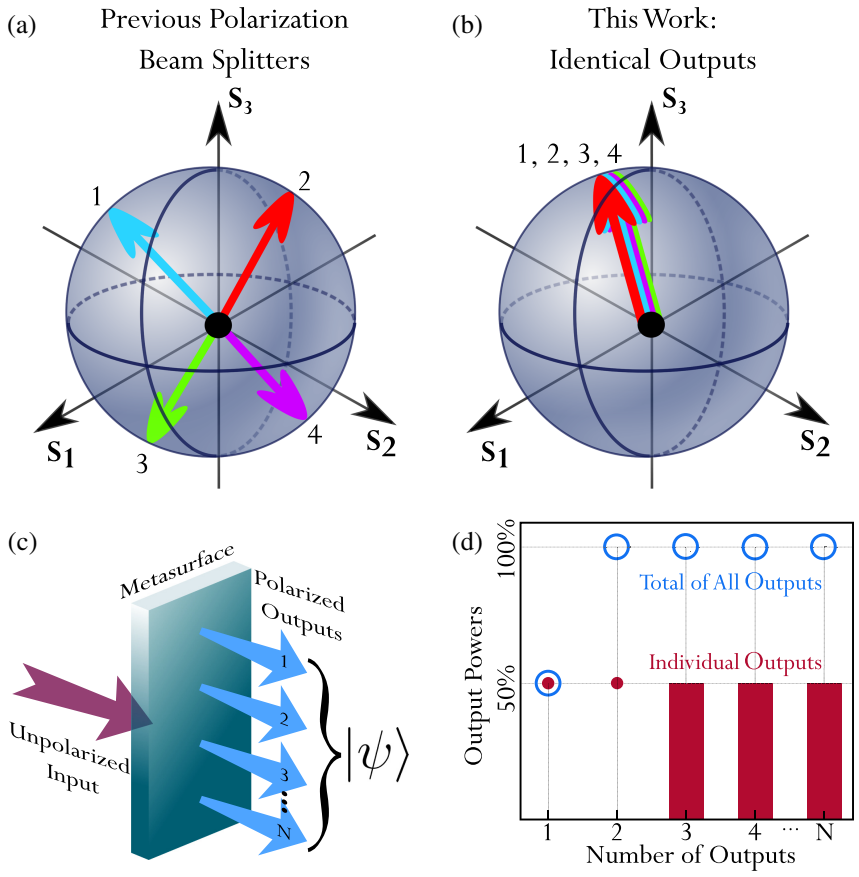

Fig. 1 Output polarization states shown on a Poincaré sphere for (a) previously realized metasurfaces that split polarizations into pairwise orthogonal states between different outputs (1 and 4, 2 and 3) and (b) the proposed metasurface, which achieves spatially uniform polarization across several outputs. (c) A schematic depicting a metasurface which converts an unpolarized input into N outputs with identical polarization states $|\psi\rangle$. (d) The permissible transmitted power of an ideal polarizer for a different number of outputs. The red markers show the allowed transmission of individual output channels, and the blue markers show the maximum total transmission of all output channels.

advances in polarization optics can improve the energy efficiency of many optical technologies employing unpolarized or partially polarized light sources.

2 Method

2.1 Deriving Fundamental Limits to Conversion Efficiency

We first formulate the general properties of any passive linear optical device with N total outputs, where an unpolarized light source is coupled to a single input port [Fig. 1(c)]. For maximum conversion efficiency of unpolarized to polarized light, we aim to fully transmit all input power across the outputs. Each output has a predefined target pure polarization state $|\psi_{1,2,\ldots,N}\rangle$. Mathematically, this transformation to an arbitrary output state $|\psi_n\rangle$ of the n^{th} output can be defined by a Jones matrix,

$$\mathbf{J}_n = A_n|\psi_n\rangle\langle\phi_n|. \tag{1}$$

The input state $|\phi_n\rangle$ is optimized to maximize the transmission efficiency, and A_n are real-valued transmission amplitudes that are bounded for passive devices as $0 \le A_n \le 1$. An input unpolarized light source can be represented as a mixed state with the density matrix

$$\rho_{\text{in}} = \frac{1}{2}(|H\rangle\langle H| + |V\rangle\langle V|). \tag{2}$$

The corresponding power transmission to each output is then $P_{\text{unpol},n} = 0.5|A_n|^2$, meaning that the maximum conversion efficiency for each output is 50% [red marker in Fig. 1(d)]. The total power efficiency is $P_{\text{unpol,total}} = 0.5\sum_{n=1}^{N}|A_n|^2$, which should be no more than unity for passive devices. Then, the general research question becomes: can we find a set of input states $|\phi_{1,2,\ldots,N}\rangle$ such that $P_{\text{unpol,total}} = 1$ for any given set of output states $|\psi_{1,2,\ldots,N}\rangle$ and arbitrary power splitting portions.

We find that full power efficiency can be achieved for $N \ge 2$, as shown by the blue markers in Fig. 1(d) and in Sec. S1 in the Supplementary Material.[35] For $N = 2$, the power transmission to each of the two outputs is exactly 50%, meaning that there is no flexibility in the power splitting when realizing 100% total efficiency. Nevertheless, in this scenario, there is still an arbitrary choice of the pure output polarization states, including having the same output polarization. In comparison, previous bulky optics and metasurface-based PBSs have never explored the full potential of a dual-output polarizer.

For three or more outputs, 100% total efficiency can be achieved with arbitrary output states and any power splitting portions, only subject to a condition that each output has a maximum of 50% power, as marked by the red shading in Fig. 1(d). After defining the output states and power splitting portions, analytical forms of the right singular states $|\phi_{1,2,3}\rangle$ can be obtained for three outputs, which are derived in Sec. S1.3 in the Supplementary Material.[35] For $N \ge 4$ output ports, there are nonunique solutions, since the number of allowed free parameters oversatisfy the necessary conditions. We present a particular analytical solution in Sec. S1.4 in the Supplementary Material.[35] We emphasize that this is a general result; a passive optical device with $N \ge 2$ ports may have 100% total efficiency in achieving arbitrary output polarization states. In addition, a device with $N \ge 3$ ports may also have arbitrary power-splitting portions at the outputs, provided that no single port contributes more than 50% to the total efficiency. Replicating the functionality of this device with a conventional optical system would require a series of multiple PBSs, wave plates, and other bulky optical elements (Sec. S2 in the Supplementary Material[35]).

2.2 Topology Optimization

We illustrate a particular case of polarization conversion by designing metagratings that split an incoming unpolarized beam into multiple diffraction orders, all having identical output-pure polarizations $|\psi_{1,2,\ldots,N}\rangle = |\psi\rangle$. This operational functionality achieves spatially uniform polarization that can be beneficial for structured illumination applications.[36] Dielectric metasurfaces are commonly and successfully designed in the framework of weakly interacting uncoupled resonators,[28,37–40] where the output fields are determined by the superposition of position-dependent transfer matrices. However, we find that this type of metasurface construction does not enable our desired functionality. Specifically, according to Eq. (6) in Ref. 28 $J_n = A_n|\phi_n^*\rangle\langle\phi_n|$, conventional nonchiral pillar-based metasurfaces are restricted to the target Jones matrices with $|\psi_n\rangle = |\phi_n^*\rangle$. It means that for identical output pure polarizations $|\psi_n\rangle = |\psi\rangle$, one necessarily has $|\phi_n\rangle = |\psi^*\rangle$. This device would filter out one input polarization component with the same output efficiency limit of 50% as a conventional polarizer.

We overcome this apparent roadblock by designing dielectric metasurfaces with a spatially nonlocal response, where the polarization transformations depend on the diffraction order. For this purpose, we perform inverse design with free-form topology optimization[41–44] by adopting the MetaNet codebase[45] in combination with RETICOLO rigorously coupled wave analysis.[46] Our figure of merit (FOM) is formulated as the difference between the transmitted target and undesired orthogonal polarization intensities, multiplied over all output diffraction orders,

$$\text{FOM} = \prod_n(|\langle\psi|\mathbf{J}_n|^2 - |\langle\psi_\perp|\mathbf{J}_n|^2), \tag{3}$$

where $|\psi\rangle$ is the desired output polarization state for all diffraction orders, and $|\psi_\perp\rangle$ is an undesired orthogonal state ($\langle\psi|\psi_\perp\rangle = 0$). By overlapping the electric fields of forward and adjoint simulations, the material derivative of the FOM is determined. The gradient information is then used as part of a gradient descent algorithm to progress the material distribution of the metasurface to an optimal point. Exact expressions for the derivative of the FOM are given in Sec. S3 in the Supplementary Material.[35]

3 Results and Discussion

3.1 Simulation Results

In the first design, we target the splitting of an incoming unpolarized beam into two outgoing beams ($N = 2$) with the same diagonal linear polarization $|D\rangle$. This can be achieved with an angled incidence of the input beam such that only two diffraction orders exist in the transmission direction [Fig. 2(a)]. We design the metasurface for equal transmitted diffraction efficiency into the $m = 0$ and $m = 1$ orders [Fig. 2(b)]. The incident angle is $\alpha = 45$ deg for the unpolarized input light. An

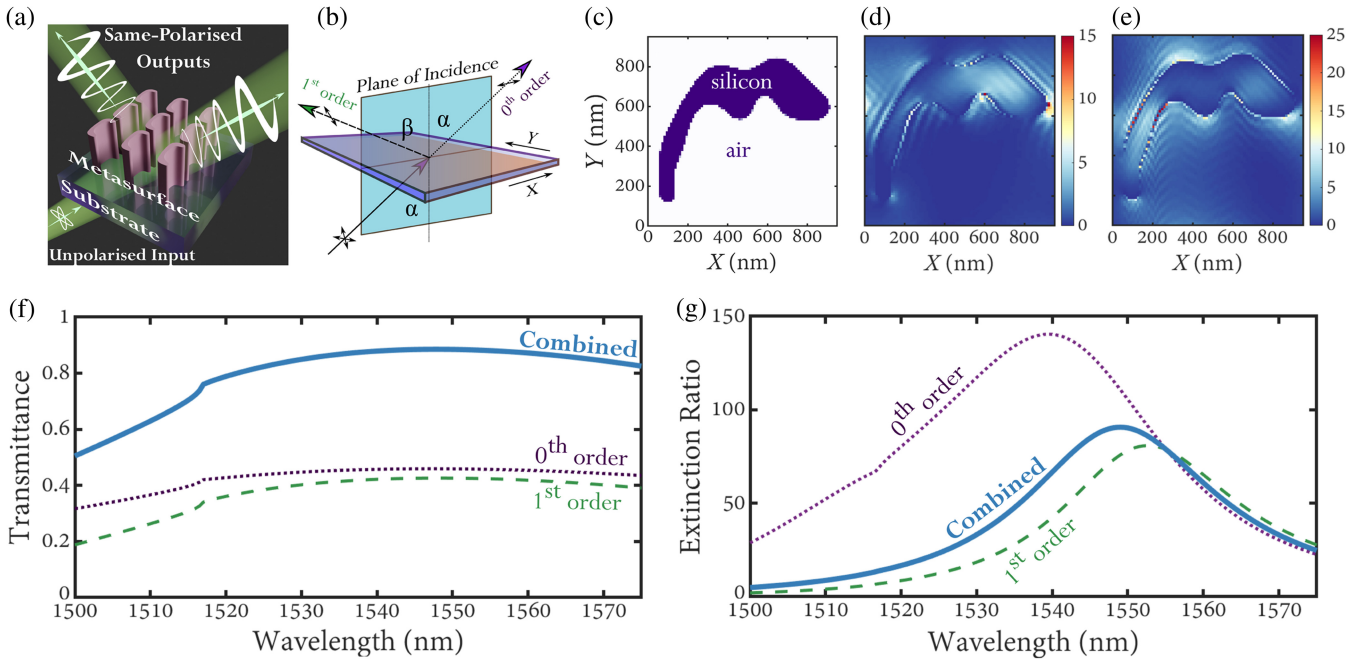

Fig. 2 (a) Illustration of the dual-output polarizing metasurface. (b) Operating scheme of the metasurface in transmission, with an incident angle of $\alpha = 45$ deg and first-order diffraction angle of $\beta = 68$ deg. (c) Final metasurface design of the single unit cell, with a period 950 nm along both directions. The shaded region represents silicon, and the void represents air. (d) Electric field intensity enhancement for incident $|H\rangle$ polarization, and (e) $|V\rangle$ polarization. These have the same unit cell dimensions as (c). (f) Predicted transmitted power, and (g) extinction ratio of the diagonal linear polarization for each diffraction order.

oblique angle of incidence is chosen for a first demonstration, which simplifies the optimization by eliminating unwanted higher-order diffraction orders. With 45 deg, the two diffraction channels are reasonably separated spatially to individually measure in an experimental setup.

We run the topology optimization starting with a random distribution of refractive indices in the unit cell. The design is based on a silicon layer ($n = 3.48$ at $\lambda = 1550$ nm) with a thickness of 1000 nm on a 460 μm sapphire substrate ($n = 1.75$ at $\lambda = 1550$ nm), corresponding to our physical sample. The algorithm also incorporates binarization of the perturbation region to either silicon or air with a constraint on minimum feature size.[47] The optimized complex shape of the nanoresonator is shown in Fig. 2(c). Due to its asymmetric shape, the localized fields induced in the resonator are highly nontrivial. For example, when the incident light is polarized in the X-direction ($|H\rangle$ polarization) [Fig. 2(d)], most of the field is concentrated on the right tip of the nanoresonator. However, when incident light is polarized in the Y-direction ($|V\rangle$ polarization) [Fig. 2(e)], the light is instead concentrated along the left arm of the nanoresonator. Therefore, the action of the metasurface on unpolarized light is defined through a complex superposition of induced fields in the nanoresonator.

The modeling predicts highly efficient conversion of unpolarized light to the target diagonal state $|D\rangle$ at both outputs [Fig. 2(f)]. The combined total efficiency is beyond 80% over an extended wavelength range of 1520 to 1570 nm. Importantly, this performance fundamentally exceeds the 50% limit of conventional polarizers, with a combined extinction ratio that approaches 100 at 1550 nm [Fig. 2(g)].

While the resulting optimized metasurface geometry delivers the required polarization transmission performance, the underlying mechanism of its operation, and the interplay between local and nonlocal modes, may not be intuitively obvious. We employ the singular value decompositions of the scattering matrix to elucidate the mechanism with which polarizations are split and rotated for different outputs (Sec. S4 in the Supplementary Material[35]). Then, to obtain physical insight, we perform multipolar decomposition[48] to identify the predominant local modes of the metasurface under different polarizations (Sec. S5 in the Supplementary Material[35]). We find that electric and magnetic dipole modes provide the strongest scattering and polarization-filtering response. At the same time, the metasurface has a nonlocal characteristic allowing for the nontrivial dependence of transmission on the diffraction orders beyond the limits of local metasurfaces, as discussed above. We provide performance comparisons to previously demonstrated metasurface polarizers and commercially available polarizers in Sec. S6 in the Supplementary Material (see also Refs. 49–51 therein). The metasurface maintains effective performance greater than the threshold 50% efficiency over the entire incident angle (α) range from 40 deg to 80 deg. Peak conversion efficiency of ~80% is reached at around 50 deg incidence, which is shown in Sec. S7 in the Supplementary Material.[35] While this work focuses on optimization of metasurfaces that are amenable to current planar silicon fabrication platforms,

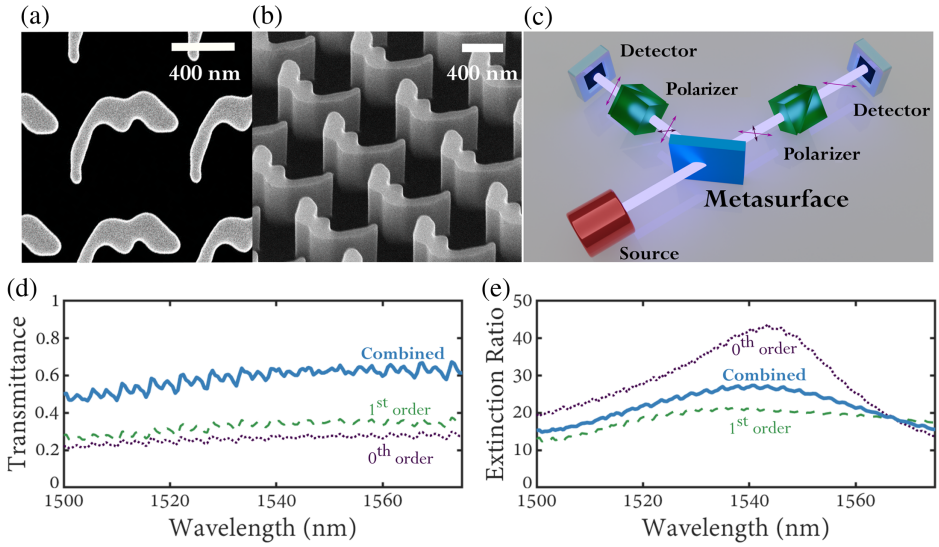

Fig. 3 (a) Top-down and (b) tilted SEM images of the fabricated metasurface. (c) Simplified experimental setup. The source transmits through the metasurface, which diffracts the beam into two orders. Each arm analyses the diagonal polarization before reaching the detector. (d) Measured transmitted power, and (e) extinction ratio of the diagonal polarization for each diffraction order for an incident angle $\alpha = 45$ deg.

new manufacturing processes in the near future may open up greater possibilities. The total efficiency can likely be increased beyond 90% with multilayer metasurfaces or volumetric metamaterials, which were shown to enhance performance in devices for different applications.[52–55]

3.2 Experimental Results

We successfully fabricate the optimized design using e-beam lithography and standard silicon etching, as shown in Figs. 3(a) and 3(b). The characterization of the metasurface was then performed in free space, where we measured the $m = 0$ and $m = 1$ diffraction orders, as illustrated in Fig. 3(c). The experiments were performed with the horizontal and vertical input polarization states in two separate measurements, mimicking the unpolarized incident light according to Eq. (2); see Sec. S8 in the Supplementary Material[35] for further details. These states were prepared from a continuous-wave tunable laser, operating in the near-infrared within the telecommunications band wavelengths of 1500 to 1575 nm. Calibration measurements against air, described in Sec. S9 in the Supplementary Material,[35] are taken to determine the variation in input power across all relevant wavelengths. These values are then used to calculate the absolute metasurface transmission efficiency.

We experimentally demonstrate the metasurface's ability to convert unpolarized light to diagonal polarized light with an absolute efficiency close to ~70% [Fig. 3(d)], exceeding the 50% limit of previous approaches. This performance is maintained across a broad wavelength range, from 1540 to 1570 nm. The extinction ratio of desired to undesired output polarization states exceeds 20 at the target wavelength of 1550 nm, see Fig. 3(e). We discuss the fabrication performance tolerances for our metasurface in Sec. S11 in the Supplementary Material.[35]

For another demonstration, we optimize for and experimentally characterize a two-output circular polarizer; see Sec. S10 in the Supplementary Material.[35] The metasurface is able to realize

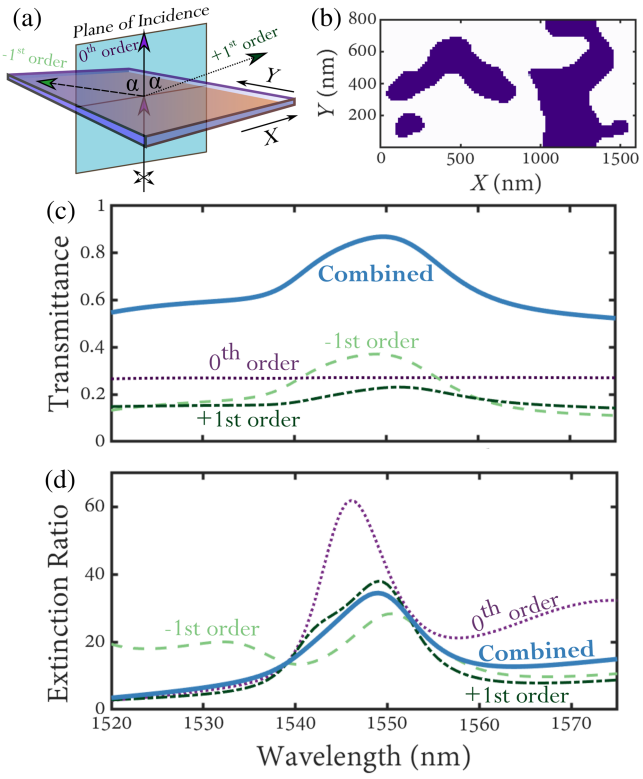

Fig. 4 (a) Operating principle of a three-output metasurface polarizer. The incident beam is normal, and $\alpha = 75$ deg. (b) The binarized metasurface pattern, with shaded regions representing silicon and the void representing air. (c) Transmittance of desired vertical polarization versus wavelength. (d) Extinction ratio of combined vertical to horizontal polarization.

conversion of unpolarized light into circularly polarized light with approximately 60% efficiency, thereby exceeding the 50% limit.

3.3 Designs for Three and More Outputs

We then extend our method to design metasurfaces that generate three or more outputs. As discussed above and visualized in Fig. 1(d), there is freedom in the distribution of output powers for more than two diffraction orders. We present a metasurface with nonequal power splitting portions for each of the three outputs [Fig. 4(a)], with the optimized design shown in Fig. 4(b). The unit cell is chosen to be 1600 nm by 800 nm. The reason for the rectangular unit cell is to avoid diffraction in air along the y direction, while only allowing first-order diffraction in the x direction. In this configuration, the zeroth order is normal to the plane of the metasurface. This three-output design realizes high combined transmittance of over 80% to the target vertical linear polarization $|V\rangle$, and an extinction ratio over $|H\rangle$ output approaching 40 at 1550 nm [Figs. 4(c) and 4(d)]. Moreover, in Sec. S12 in the Supplementary Material,[35] we show a nontrivial metasurface design where incoming unpolarized light is split into four outputs with the same polarization while achieving similar performance.

It is instructive to discuss a question on whether it is possible to recombine the multiple output beams into one. Fundamentally, for two-output splitting, the beams are mutually incoherent and cannot be recombined coherently with any passive device. However, for three of more outputs, the beams can be partially spatially coherent. There is potential in future work to explore different beam recombination schemes and utilize them for further tailoring different structured light and dot projection schemes.

4 Conclusion

We anticipate that metasurfaces facilitating highly efficient shaping of unpolarized light into uniformly polarized outputs will find various applications, including polarized imaging with basic unpolarized sources from LED and multimode lasers. Our multi-output devices achieve this functionality in a single-layer metasurface, dramatically reducing the footprint required. Our results also demonstrate that nontrivial combinations of local and nonlocal resonances in topologically optimized metasurfaces can overcome limitations associated with arrays of weakly coupled resonators, thereby opening a path to broader polarization manipulation functionalities.

Code and Data Availability

Code and Data related to obtaining the results presented in this paper may be reasonably requested from the authors.

Acknowledgments

We acknowledge the support of the Australian Research Council (Grant Nos. NI210100072, LP180100904, and CE200100010). This work was performed in part at the Melbourne Centre for Nanofabrication (MCN) in the Victorian Node of the Australian National Fabrication Facility (ANFF).

References

1. J. C. Ramella-Roman, I. Saytashev, and M. Piccini, "A review of polarization-based imaging technologies for clinical and preclinical applications," *J. Opt.* **22**(12), 123001 (2020).
2. M. P. Row et al., "Polarization-difference imaging: a biologically inspired technique for observation through scattering media," *Opt. Lett.* **20**(6), 608–610 (1995).
3. Z. Nan et al., "Linear polarization difference imaging and its potential applications," *Appl. Opt.* **48**(35), 6734–6739 (2009).
4. L. Yan et al., "General review of optical polarization remote sensing," *Int. J. Remote Sens.* **41**, 4853–4864 (2020).
5. L. Yan et al., *Polarization Remote Sensing Physics*, Springer Nature, Singapore (2020).
6. J. N. Damask, *Polarization Optics in Telecommunications*, Vol. 101 of Springer Series in Optical Sciences, Springer-Verlag, New York (2004).
7. C. Guo et al., "Advances on exploiting polarization in wireless communications: channels, technologies, and applications," *IEEE Commun. Surv. Tutorials* **19**(1), 125–166 (2017).
8. X. Huang et al., "Polarization structured light 3D depth image sensor for scenes with reflective surfaces," *Nat. Commun.* **14**(1), 6855 (2023).
9. E. Matioli et al., "High-brightness polarized light-emitting diodes," *Light Sci. Appl.* **1**, e22 (2012).
10. J. Y. Wang et al., "Polarized light-emitting diodes based on anisotropic excitons in few-layer ReS2," *Adv. Mater.* **32**, 2001890 (2020).
11. J. P. Huang et al., "Linearly polarized light emission from GaN micro-LEDs for 3D display," *Appl. Phys. Lett.* **122**, 111107 (2023).
12. M. Chekhova and P. Banzer, *Polarization of Light in Classical, Quantum, and Nonlinear Optics*, De Gruyter, Berlin (2021).
13. E. Collett, *Field Guide to Polarization*, SPIE Press, Bellingham, Washington (2005).
14. A. V. Kildishev, A. Boltasseva, and V. M. Shalaev, "Planar photonics with metasurfaces," *Science* **339**(6125), 1232009 (2013).
15. O. Quevedo-Teruel et al., "Roadmap on metasurfaces," *J. Opt.* **21**, 073002 (2019).
16. S. Lung et al., "Complex-birefringent dielectric metasurfaces for arbitrary polarization-pair transformations," *ACS Photonics* **7**, 3015–3022 (2020).
17. J. P. B. Mueller et al., "Metasurface polarization optics: independent phase control of arbitrary orthogonal states of polarization," *Phys. Rev. Lett.* **118**, 113901 (2017).
18. A. Cerjan and S. H. Fan, "Achieving arbitrary control over pairs of polarization states using complex birefringent metamaterials," *Phys. Rev. Lett.* **118**, 253902 (2017).
19. Y.-J. Gao et al., "Simultaneous generation of arbitrary assembly of polarization states with geometrical-scaling-induced phase modulation," *Phys. Rev. X* **10**, 31035 (2020).
20. J. Hong et al., "Nonlocal metasurface for circularly polarized light detection," *Optica* **10**(1), 134–141 (2023).
21. S. Wang et al., "Arbitrary polarization conversion dichroism metasurfaces for all-in-one full Poincaré sphere polarizers," *Light Sci. Appl.* **10**(1), 24 (2021).
22. F. Ding et al., "Versatile polarization generation and manipulation using dielectric metasurfaces," *Laser Photonics Rev.* **14**, 2000116 (2020).
23. Y. Q. Hu et al., "All-dielectric metasurfaces for polarization manipulation: principles and emerging applications," *Nanophotonics* **9**, 3755–3780 (2020).
24. A. H. Dorrah et al., "Metasurface optics for on-demand polarization transformations along the optical path," *Nat. Photonics* **15**(4), 287–296 (2021).
25. X. Q. Zhang et al., "Direct polarization measurement using a multiplexed Pancharatnam-Berry metahologram," *Optica* **6**, 1190–1198 (2019).
26. E. Arbabi et al., "Full-Stokes imaging polarimetry using dielectric metasurfaces," *ACS Photonics* **5**, 3132–3140 (2018).

27. S. Gao et al., "Efficient all-dielectric diatomic metasurface for linear polarization generation and 1-bit phase control," *ACS Appl. Mater. Interfaces* **13**, 14497–14506 (2021).
28. N. A. Rubin et al., "Jones matrix holography with metasurfaces," *Sci. Adv.* **7**(33), eabg7488 (2021).
29. S. Wang et al., "Metasurface-based solid poincare sphere polarizer," *Phys. Rev. Lett.* **130**, 123801 (2023).
30. Q. Zhang et al., "Design of beam deflector, splitters, wave plates and metalens using photonic elements with dielectric metasurface," *Opt. Commun.* **411**, 93–100 (2018).
31. B. Wang et al., "Rochon-prism-like planar circularly polarized beam splitters based on dielectric metasurfaces," *ACS Photonics* **5**, 1660–1664 (2018).
32. M. Khorasaninejad, W. Zhu, and K. B. Crozier, "Efficient polarization beam splitter pixels based on a dielectric metasurface," *Optica* **2**, 376–382 (2015).
33. B. A. Slovick et al., "Metasurface polarization splitter," *Philos. Trans. R. Soc. A Math. Phys. Eng. Sci.* **375**, 20160072 (2017).
34. R. Zhao et al., "Controllable polarization and diffraction modulated multi-functionality based on metasurface," *Adv. Opt. Mater.* **10**, 2102596 (2022).
35. "See Supplemental Material at [URL will be inserted by publisher] for further details in mathematical derivations, metasurface simulations, and experiments".
36. Y. B. Ni et al., "Metasurface for structured light projection over 120 degrees field of view," *Nano Lett.* **20**, 6719–6724 (2020).
37. S. M. Kamali et al., "A review of dielectric optical metasurfaces for wavefront control," *Nanophotonics* **7**(6), 1041–1068 (2018).
38. W. T. Chen, A. Y. Zhu, and F. Capasso, "Flat optics with dispersion-engineered metasurfaces," *Nat. Rev. Mater.* **5**(8), 604–620 (2020).
39. N. Yu and F. Capasso, "Flat optics with designer metasurfaces," *Nat. Mater.* **13**(2), 139–150 (2014).
40. Y. Qiu et al., "Fundamentals and applications of spin-decoupled Pancharatnam—Berry metasurfaces," *Front. Optoelectron.* **14**(2), 134–147 (2021).
41. J. A. Fan, "Freeform metasurface design based on topology optimization," *MRS Bull.* **45**, 196–201 (2020).
42. Z. J. Shi et al., "Continuous angle-tunable birefringence with freeform metasurfaces for arbitrary polarization conversion," *Sci. Adv.* **6**, eaba3367 (2020).
43. J. S. Jensen and O. Sigmund, "Topology optimization for nano-photonics," *Laser Photonics Rev.* **5**, 308–321 (2011).
44. Z. Li et al., "Empowering metasurfaces with inverse design: principles and applications," *ACS Photonics* **9**, 2178–2192 (2022).
45. J. Q. Jiang et al., "Metanet: a new paradigm for data sharing in photonics research," *Opt. Express* **28**, 13670–13681 (2020).
46. J. P. Hugonin and P. Lalanne, "RETICOLO software for grating analysis," arXiv 2101.00901 (2021).
47. E. W. Wang et al., "Robust design of topology-optimized metasurfaces," *Opt. Mater. Express* **9**(2), 469–482 (2019).
48. R. Alaee, C. Rockstuhl, and I. Fernandez-Corbaton, "An electromagnetic multipole expansion beyond the long-wavelength approximation," *Opt. Commun.* **407**, 17–21 (2018).
49. H. Hemmati, P. Bootpakdeetam, and R. Magnusson, "Metamaterial polarizer providing principally unlimited extinction," *Opt. Lett.* **44**(22), 5630–5633 (2019).
50. H. Kurosawa et al., "High-performance metasurface polarizers with extinction ratios exceeding 12000," *Opt. Express* **25**(4), 4446–4455 (2017).
51. S. Vandendriessche, Polarizer Selection Guide, Edmund Optics, https://www.edmundoptics.com/knowledge-center/application-notes/optics/polarizer-selection-guide/ (accessed 8 September 2024).
52. C. Roques-Carmes et al., "Toward 3D-printed inverse-designed metaoptics," *ACS Photonics* **9**, 43–51 (2022).
53. M. Mansouree et al., "Multifunctional 2.5D metastructures enabled by adjoint optimization," *Optica* **7**(1), 77–84 (2020).
54. Z. Shi et al., "Nonseparable polarization wavefront transformation," *Phys. Rev. Lett.* **129**, 167403 (2022).
55. G. Roberts et al., "3D-patterned inverse-designed mid-infrared metaoptics," *Nat. Commun.* **14**(1), 2768 (2023).
56. W. R. Clements et al., "Optimal design for universal multiport interferometers," *Optica* **3**(12), 1460–1465 (2016).
57. B. A. Bell and I. A. Walmsley, "Further compactifying linear optical unitaries," *APL Photonics* **6**, 070804 (2021).

Neuton Li is a PhD candidate at the Australian National University (ANU) and the Centre of Excellence for Transformative Meta-Optical Systems (TMOS). He obtained his MSc and BSc degrees from University of Melbourne. Previously, he was a Fulbright Scholar at the California Institute of Technology. His main research interests lie in topology optimization and inverse design of optical metasurfaces.

Jihua Zhang is a researcher in Songshan Lake Materials Laboratory. Before joining Songshan Lake Materials Laboratory in 2024, he was a research fellow in the TMOS at Australian National University. He obtained dual PhD degrees from University Paris-Saclay and Huazhong University of Science and Technology in 2016. His research focuses on metasurfaces and integrated circuits for quantum photonics.

Shaun Lung received his doctorate degree from the ANU in 2022, with a focus on polarization manipulation and measurement using metasurfaces, working primarily in experimental and computational aspects. He is working as a postdoctoral researcher at Friedrich Schiller Universität, Germany, in 2023. His interests remain within both computational and experimental optics, with a strong inclination toward metasurface development.

Dragomir N. Neshev is a professor of physics at the ANU and director of the ARC Centre of Excellence for Transformative Meta-Optical Systems. He received his PhD in physics from Sofia University in 1999. He leads the Experimental Photonics Group at ANU and has made significant contributions to optics, including pioneering dielectric meta-optics and nonlinear metasurfaces. He is a fellow of Optica and a member of SPIE.

Andrey A. Sukhorukov is a professor at the Research School of Physics of the ANU and a member of the TMOS Centre. He leads a research group on nonlinear and quantum photonics, targeting the fundamental aspects of the miniaturization of optical elements down to micro- and nanoscale. In 2015, he was elected a fellow of Optica for contributions to nonlinear and quantum-integrated photonics, including frequency conversion and broadband light manipulation in waveguide circuits and metamaterials.